GeoConvention 2015
GEOSCIENCE
new horizons
Telus Convention Centre • 4-8 May 2015 • Calgary, AB Canada

Analytical Stress Modeling for Mine related Microseismicity

Himanshu Barthwal and Mirko van der Baan
University of Alberta

Summary

Microseismicity is recorded in an underground mine by a network of 7 boreholes each having 4 geophones during January 2011. The inverted event locations are confined in a narrow band between depths of 0.4 to 0.5 km around the tunnels. We propose a simplified geomechanical model for the tunnels as an oblate spheroidal cavity and compute stress concentration around it using Eshelby's equivalent inclusion method. We use Coulomb's failure function as a stability criterion to identify regions most susceptible to shear slippages which show good match with the observed microseismic cloud. The same methodology is in principle applicable to microseismic data recorded during hydraulic fracturing treatments and may give more insight into the possible shape of the induced fracture network, resulting stress changes and the recorded microseismic cloud.

Introduction

Microseismic monitoring is being used increasingly in assessing the safety and progress of underground mining operations (Young and Maxwell, 1992; Westman et al., 2012; Castellanos and Van der Baan, 2014). Most of the applications involve locating and tracking microseismic events. Microseismic data in exploration settings usually contain many events with similar waveform. Waveform crosscorrelation techniques have been used to compute highly accurate differential arrival times and accurate relative relocations (Poupinet et al., 1984; Waldhauser and Ellsworth, 2000; Castellanos and Van der Baan, 2013). The higher accuracy in event locations allows for advanced geomechanical interpretation of the overall process causing microseismicity.
We analyze the relocated microseismic events around tunnels in an underground mine by modeling the tunnels as oblate spheroidal cavity and computing stress concentrations around it. The spheroidal cavity leads to differential stress concentrations in the surrounding rock mass which cause some regions to fail more likely than others. Our modeled results show good match with the observed relocated microseismic events cloud.

Background data

In order to monitor zones of potential instabilities and possible water inflow incidents, a microseismic system was installed in an underground mine. A network of 7 monitoring wells each with 4 active three-components geophones recorded the microseismic events during January 2011. Castellanos and Van der Baan (2013) relocated these microseismic events using double-difference relocation. Barthwal and Van der Baan (2014) performed double-difference tomography on this dataset to simultaneously invert for event locations and velocity model. Figure 1 shows the relocated microseismic events overlying the inverted velocity model and tunnel layout which are strongly clustered towards the center of the modeled region at X=0.2 km, Y=0.2 km between depths of 0.4 km to 0.5 km. Castellanos and Van der Baan (2014) concluded that this microseismicity is not related with blasting activities in the mine but might have been triggered by the transportation of the debris.

Stress modeling

The tunnels have extensive areal coverage (Figure 1) so we can model them as an oblate spheroid with semi major axes a, b and c along X, Y and Z axes respectively such that a=b >>c. From well bore stress measurements, we know that the minimum principal stress is 0.87 of the vertical stress and the maximum principal stress is 1.15 of the vertical stress for a rock mass with a saturated density of 2,500 kg/m^3.

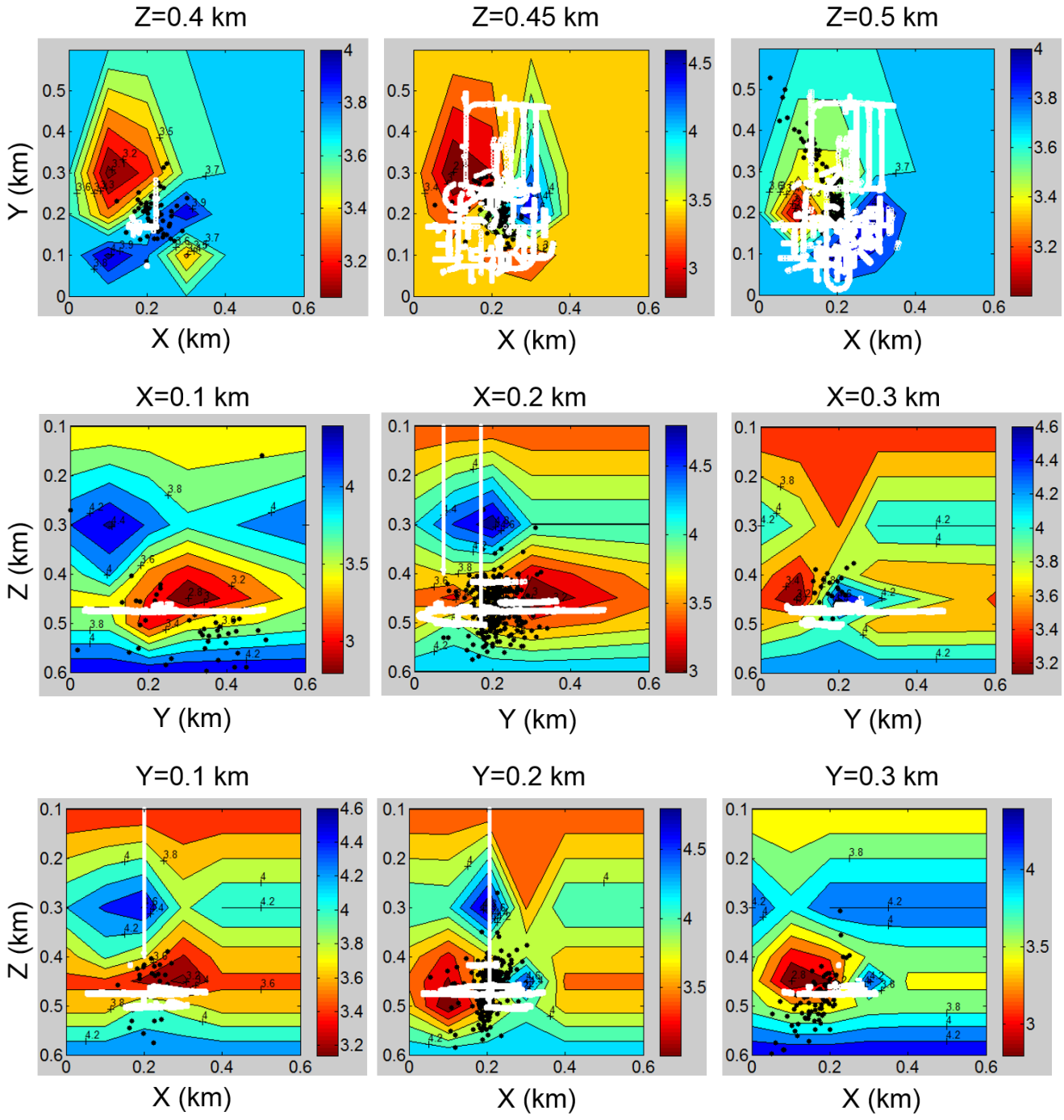

Figure 1: Inverted event locations overlying the tunnel layout and inverted velocity model obtained from double difference tomography. Top: Map view at depths of 0.4 km, 0.45 km and 0.5 km. Middle: North-South cross section at X=0.1 km, 0.2 km and 0.3 km. Bottom: East-West cross section at Y=0.1 km, 0.2 km and 0.3 km. The events show strong clustering around X=0.2 km, Y=0.2 km between depths of 0.4 to 0.5 km. The tunnels have extensive areal coverage as observed in the map view (top panel).

Table 1 shows the parameters of the oblate spheroid used to compute stress concentration. We assume that the far field principal stresses are uniform. We use Eshelby's equivalent inclusion method (Eshelby, 1957; Ju and Sun, 2001; Healy, 2009) for finding the stresses outside the spheroidal cavity. The stress perturbations outside a spheroidal cavity centered at x^1 is given by

$$\boldsymbol{\sigma}' = [\mathbf{C_0}.\mathbf{G}(x - x^1)]:\boldsymbol{\varepsilon}^* \quad (1)$$

where $\mathbf{C_0}$ is the linear elasticity tensor, $\mathbf{G}(x-x^1)$ is the exterior point Eshelby's tensor and $\boldsymbol{\varepsilon}$ is the non-interacting eigen strain. The explicit mathematical expressions for $\mathbf{G}(x-x^1)$ and $\boldsymbol{\varepsilon}$ can be found in Ju and Sun (2001). For an isotropic medium, the linear elasticity tensor $\mathbf{C_0}$ contains only two independent elastic constants.

Since the spheroidal cavity leads to differential stress concentrations in the surrounding rock mass, there are some regions which are more likely to fail as compared to others. To analyze the stability around the cavity, we determine the Coulomb failure factor (CFF) as

$$CFF = \boldsymbol{\tau} - \mu\boldsymbol{\sigma}_n \quad (2)$$

where $\boldsymbol{\tau}$ and $\boldsymbol{\sigma}_n$ are the shear and normal stresses respectively acting on any weakness plane with a given orientation and μ is the coefficient of friction. We assume zero cohesive strength and take μ=0.6 owing to the presence of pre-existing fractures. Then CFF>0 represents the regions which are most likely to undergo shear slippages under the prescribed stresses (Zoback, 2007). We compute the normal and shear stresses on an arbitrary plane whose normal makes equal angles with the three principal axes such that its components $n_1=n_2=n_3=\frac{1}{\sqrt{3}}$. This plane will have the maximum shear stress under given principal stresses. The normal stress $\boldsymbol{\sigma}_n$ and the shear stress $\boldsymbol{\tau}$ on this plane are computed as

$$\boldsymbol{\sigma}_n = n_1^2\,\boldsymbol{\sigma}_1 + n_2^2\,\boldsymbol{\sigma}_2 + n_3^2\,\boldsymbol{\sigma}_3 = (\boldsymbol{\sigma}_1 + \boldsymbol{\sigma}_2 + \boldsymbol{\sigma}_3)/3 \quad (3)$$

$$\boldsymbol{\tau} = n_1^2\,\boldsymbol{\sigma}_1^2 + n_2^2\,\boldsymbol{\sigma}_2^2 + n_3^2\,\boldsymbol{\sigma}_3^2 = [(\boldsymbol{\sigma}_1^2 + \boldsymbol{\sigma}_2^2 + \boldsymbol{\sigma}_3^2)/3] - \boldsymbol{\sigma}_n^2 \quad (4)$$

where $\boldsymbol{\sigma}_1$, $\boldsymbol{\sigma}_2$ and $\boldsymbol{\sigma}_3$ are the near field stresses resulting from the sum of the uniform far field stresses and the stresses concentrated around the spheroidal cavity computed using Eshelby's equivalent inclusion method.

Depth, h (m)	a (m)	b (m)	c (m)	Density, ρ kg/m^3	Lame parameter, λ (GPa)	Poisson's ratio, nu	Vertical stress, $\boldsymbol{\sigma}_v$
475	100	100	15	2500	17.5	0.2	ρgh

Table 1: Parameters for computing stress concentration around the oblate spheroid.

Results

Figure 2a-c shows the stress perturbations around an oblate spheroid computed in a vertical cross section along the maximum horizontal stress passing through the center of the spheroid. The stress perturbations in the normal horizontal stresses is extensional in the region above and below the center while it is compressional along the equator. The cavity does not support any stress normal to its surface, so the horizontal stresses normal to the cavity are zero at its surface. The vertical stress has a large compressional value along the equator, however this stress concentration is limited very close to the surface of the cavity. The vertical stress above and below the cavity is not much affected by the presence of the cavity except at its surface. The Coulomb failure factor computed around the spheroidal cavity is shown in Figure 2d. The region above and below the center of the spheroid is most unstable due to positive values of Coulomb failure factor. Since we have tunnels at depths of 420 m, 465 m, 480 m and 500 m, each one can be independently modeled as an oblate spheroid. Therefore the instability at the roof and base of a single spheroidal cavity can be further amplified due to its stress interactions with the spheroids above and below it. This model predicts a linear pattern of events clustered in a narrow region around the center of the spheroids (assumed to be at X=0.2 and Y=0.2 km) extending vertically as observed in Figure 1. Further We observe that the seismicity is clustered only around the main shaft and it is completely absent around the second shaft (Figure 1, middle panel) which suggests that the hoop stresses are not the major factor causing microseismicity.

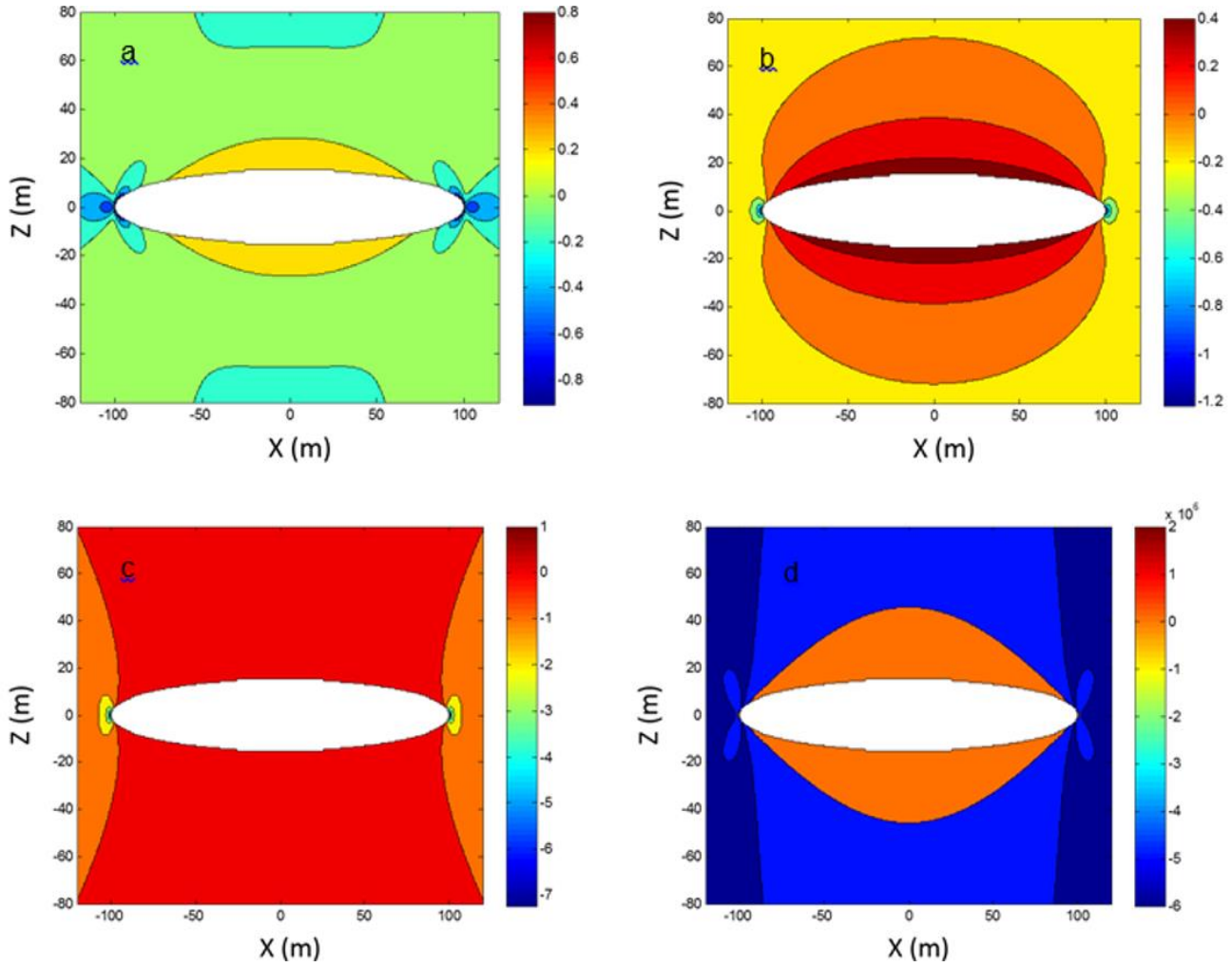

Figure 2: Vertical cross section along the maximum horizontal stress passing through the center showing stresses (a-c) and Coulomb failure function (CFF) (d) around an oblate spheroid computed with parameters given in table 1. Positive values represent tensile stresses while negative values correspond to compressive stresses (a) Relative change in normal stress along X-axis (maximum horizontal stress), (b) Relative change in normal stress along Y-axis (minimum horizontal stress), (c) Relative change in normal stress along Z-axis (vertical stress), and (d) Coulomb failure function (CFF). The roof and base of the cavity has positive CFF values and hence are prone to shear slippages.

Conclusions

We modeled the tunnels in an underground mine as oblate spheroidal cavities and computed stress concentrations around them using Eshelby's equivalent inclusion method. Using Coulomb failure function as a stability criterion we are able to identify zones prone to shear slippages which show good correlation with the inverted microseismic event locations. This analytical stress modeling is useful in identifying anomalous stress concentrations and potential sites for future microseismicity. The same methodology also holds promise for microseismic data acquired during hydraulic fracturing treatments, where the Coulomb failure function should correlate to the shape of the microseismic cloud.

Acknowledgements

We are grateful to Fernando Castellanos for preprocessing of the microseismic dataset. We would also like to thank an anonymous company for permission to use and show the dataset, and the sponsors of the Microseismic Industry Consortium for project funding.

References

Barthwal H. and M. Van der Baan, 2014, Passive seismic tomography using recorded microseismicity, SEG Technical Program Expanded Abstracts, 2357-2362.

Castellanos F. and M. Van der Baan, 2014, Dynamic triggering of microseismicity in a mine setting, GeoConvention, Calgary.

Castellanos, F., and M. Van der Baan, 2013, Microseismic event locations using the double-difference algorithm: CSEG Recorder, 38(3), 26–37.

Eshelby, J. D., 1957, The Determination of the Elastic Field of an Ellipsoidal Inclusion, and Related Problems: Proceedings of the Royal Society of London, Series A, Mathematical and Physical Sciences, 241(1226), 376-396.

Healy, D., 2009, Elastic field in 3D due to a spheroidal inclusion-MATLAB code for Eshelby's solution: Computers & Geosciences, 35, 2170-2173

Ju, J. W., and L. Z. Sun, 2001, Effective elastoplastic behavior of metal matrix composites containing randomly located aligned spheroidal inhomogeneities. Part I: micromechanics- based formulation: International Journal of Solids and Structures, 38, 182-201.

Poupinet, G., W. L. Ellsworth, and J. Frechet, 1984, Monitoring velocity variations in the crust using earthquake doublets: An application to the Calaveras Fault, California: Journal of Geophysical Research, 89, 5719–5713.

Waldhauser, F., and W. L. Ellsworth, 2000, A double-difference earthquake location algorithm: method and application to the Hayward fault: Bulletin of the Seismological Society of America, 90, 1353–1368.

Westman, E., K. Luxbacher and S. Schafrik, 2012, Passive seismic tomography for three-dimensional time-lapse imaging of mining-induced rock mass changes: The Leading Edge, 31(3), 338–345.

Young, R. P., and S. C. Maxwell, 1992, Seismic Characterization of a Highly Stressed Rock Mass Using Tomographic Imaging and Induced Seismicity: Journal of Geophysical Research, 97, 12361–12373.

Zoback, M. D., 2007, Reservoir geomechanics. Cambridge, New York: Cambridge University Press.